INNOVATION FOREVER
Open Access

Innovation Discovery
ISSN 2959-5150 (Online)

Research Article

Enhancing Oxygen Evolution Reaction through In Situ Electrochemical Oxidation for the Structural Control of Co-Fe Prussian Blue Analogue

Yajuan Chen[1], Jing Tang[1], Weijun Li[1*], Jielei Tu[2], Chao Huang[2,3*]

[1]*School of Mechanical Engineering, Liaoning Petrochemical University, Fushun, Liaoning Province, China*
[2]*Yunnan Provincial Rural Energy Engineering Key Laboratory, Yunnan Normal University, Kunming, Yunnan Province, China*
[3]*Department of Physics, City University of Hong Kong, Tat Chee Avenue, Kowloon, Hong Kong, China*

[*]***Correspondence to: Weijun Li,*** *School of Mechanical Engineering, Liaoning Petrochemical University, Fushun 113001, Liaoning Province, China; E-mail: liweijun@lnpu.edu.com;*
Chao Huang, PhD, Professor, *Department of Physics, City University of Hong Kong, Tat Chee Avenue, Kowloon, 999077, Hong Kong, China; E-mail: chuang46-c@my.cityu.edu.hk*

Abstract

The development of exceptionally efficient catalysts for the oxygen evolution reaction (OER) and gaining a deep understanding of their activity is essential for advancing electrochemical conversion technologies. Prussian blue analogues (PBAs) serve as promising pre-catalysts for the OER. However, PBAs, typically prepared through the conventional co-precipitation method, exhibit a lower active site density and limited electrical transport, making them suitable precursors for the derivation of PBA derivatives. In this research, we identified a significant enhancement in the electrocatalytic performance of Co-Fe Prussian blue analogue (CoFe PBA) through electrochemical oxidation. The cubic CoFe PBA was synthesized by one-step co-precipitation method using adjusting the amount of sodium citrate and potassium ferricyanide. After the electrochemical treatment, CoFe PBA demonstrates remarkable attributes, including a low overpotential of 331mV at a current density of 10mA·cm^{-2}, a small Tafel slope of 50.4mV·dec^{-1}, and excellent long-term stability during electrolysis in a 1M KOH alkaline medium for over 37h. Moreover, the electrochemical oxidation of CoFe PBA was comprehensive, employing techniques such as Transmission electron microscope, Powder X-ray diffraction, and X-ray photoelectron spectroscopy. These analyses confirmed the presence of real active substances, including CoOOH and a part of FeOOH species, further supporting the observed improvements in electrocatalytic activity.

Keywords: Prussian blue analogues, electrochemical oxidation, structural control, oxygen evolution reaction

Received: November 24, 2023
Revised: January 22, 2024
Accepted: February 4, 2024
Published: March 15, 2024

Citation: Chen Y, Tang J, Li W, Tu J, Huang C. Enhancing Oxygen Evolution Reaction through In Situ Electrochemical Oxidation for the Structural Control of Co-Fe Prussian Blue Analogue. *Innov Discov*, 2024; 1(1): 5.

1 INTRODUCTION

In recent years, the field of hydrogen energy has experienced an unprecedented surge in growth, driven by the increasing adoption of clean energy and the advancing maturity of hydrogen energy technology[1]. One prominent avenue within this field is the production of hydrogen through water electrolysis. This method is firmly established and characterized by a straightforward procedure, environmental friendliness, and the generation of high-purity gas[2]. The water electrolysis revolves around two pivotal processes: the oxygen evolution reaction (OER) and the hydrogen evolution reaction (HER)[3]. In addition, the OER process is a sluggish reaction kinetics compared to HER due to the four-electron reaction[4]. To enhance the efficiency and catalytic performance of water-splitting, researchers often introduce electrocatalysts based on materials such as IrO_2/RuO_2 and Pt/C into the reaction process[5,6]. These catalysts serve to lower the energy barrier associated with these reactions, thereby improving their overall

effectiveness[7,8]. Nonetheless, precious metals present certain drawbacks, including limited reserves and high costs, rendering them less than ideal for catalyst applications. Consequently, the use of non-precious metal catalysts as a viable alternative to precious metals has been the most common strategy for water electrolysis in these hydrogen production technologies[9-11].

Prussian blue analogs (PBAs) are comprised of metal ions core linked by organic cyanide molecules. They offer several advantages, including cost-effectiveness, ease of synthesis, an open structural framework, and the ability to tailor their composition[12]. In addition, PBAs and their derivatives show promise as catalysts for OER. They offer advantages such as affordability, a straightforward synthesis, scalability, and the ability to tailor the metal species used in the catalyst[13]. In recent years, substantial efforts have been dedicated to enhancing the electrical conductivity and catalytic activity of Co-Fe Prussian blue analogue (CoFe PBA) by introducing dopants and conductive carriers. For instance, Lu et al.[14] devised a straightforward solvothermal method to design nano-cubes of Co^{3+}-enriched CoFe Prussian blue analogs, coated with precisely controlled MoS_2 shell heterostructures, to serve as efficient OER electrocatalysts. Zeng et al.[15] have reported a novel approach in which they introduce a low Pt species content to augment the electrocatalytic activity of CoFe PBA. This enhancement is achieved through a sequence involving ammonia etching followed by calcination. García et al.[16] synthesized the Cobalt hexacyanoferrate supported on Sb-doped SnO_2, which exhibited excellent electrochemical activity with a current density of 50-100mA·cm^{-2} at a 2V cell voltage. Zhao et al.[17] successfully synthesized nanosheets of Mo-doped CoFe layered double hydroxides (Mo-doped CoFe LDH/NF) through an electrochemical transformation process. This process involved the conversion of Mo-doped CoFe Prussian blue nanocubes situated on a nickel foam substrate (Mo-doped CoFe PBA/NF)[17]. The resulting material demonstrates exceptional efficiency in facilitating overall water-splitting. In some articles, it is assumed that PBA materials have a well-defined chemical structure and readily accessible active sites under electrochemical conditions. An exceptional catalytic performance is observed in tests, and performance is further enhanced through complex preparation processes such as ion doping and microstructure design. Nonetheless, unlike the extensive research focused on doping CoFe PBA, there have been very few confirmed reports regarding the direct utilization of CoFe PBA as electrocatalysts. Herein, we raise the question of whether a different reaction mechanism exists. In this regard, relative to oxides and (oxy) hydroxides, in situ studies on these systems are rare.

In this paper, we propose a straightforward and effective method to enhance the electrocatalytic activity of CoFe PBA. This method involves the direct in situ oxidation of CoFe PBA to create metal–(oxygen) hydroxide species on PBA's surface while coordinating the unsaturated metal centers. CoFe PBA exhibited remarkable improvements through electrochemical modification, requiring only a minimal overpotential of 331mV to achieve a geometric current density of 10mA·cm^{-2}. The Tafel slope was significantly reduced to 50.4mV·dec^{-1}, surpassing the catalytic performance of the original CoFe PBA. Furthermore, this enhanced performance was sustained over a continuous 37h operation, highlighting the exceptional durability of the electrochemically modified CoFe PBA. In addition, after the electrochemical treatment, CoFe PBA was reconstructed to CoOOH and FeOOH species which are real active site for OER.

2 EXPERIMENTAL METHODS

2.1 Preparation

The synthesis process began by measuring 6mmol of Co $(NO_3)_2$ and 12mmol of sodium citrate, which were placed into a centrifuge tube. Subsequently, 80mL of deionized water was added to create what we will refer to as "solution A." In parallel, 5mmol of $K_3Fe(CN)_6$ was measured and placed into another centrifuge tube. To this, 80mL of deionized water was added, creating "solution B." Next, solution B was carefully poured into solution A, and the two solutions were thoroughly mixed and stirred for a duration of 30min. Following this mixing step, the resulting mixture was allowed to stand undisturbed for a period of 24h. Then, the mixture was subjected to centrifugation. Finally, the centrifuged material was freeze-dried, resulting in the formation of a solid CoFe PBA powder; the Fe-PBA was obtained using the same method.

A total of 0.6g of $CoCl_2·6H_2O$ (Aladdin, 98%) was introduced to the aforementioned solution and vigorously stirred for 15min at 10℃. Subsequently, $NH_3·H_2O$ (Aladdin, 28-30%) was added until the solution reached a pH of 9. Following three hours of stirring, the resulting $Co(OH)_2$ precipitate was isolated via centrifugation at 10,000rpm, followed by a thorough washing with deionized water and ethanol.

2.2 Characterization

Powder X-ray diffraction (XRD) patterns (Cu Kα, λ=1.5406A) were measured with a BRUKER D8 ADVANCE. The chemical states of the elements in the prepared products were obtained by X-ray photoelectron spectroscopy (XPS, ESCALAB). Transmission electron microscope (TEM) (JEM-2100F) and scanning electron microscope (SEM) (SU8010) were used to examine the morphology and size of the CoFe PBA nanocubes.

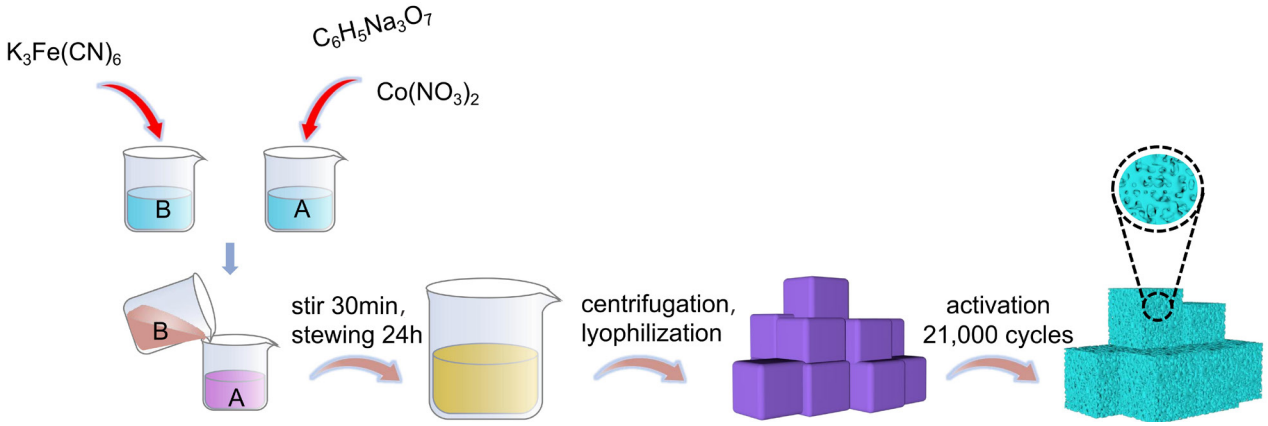

Figure 1. The schematic diagram of preparation of CoFe PBA.

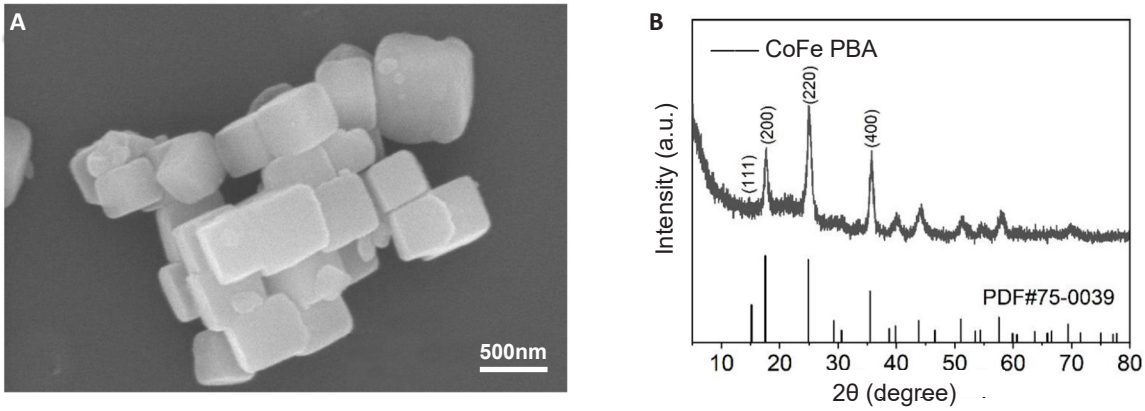

Figure 2. Image of CoFe PBA. A: SEM image of CoFe PBA. B: XRD pattern of CoFe PBA.

2.3 Electrochemical Measurements

The activity evaluation tests for OER were performed in saturated potassium hydroxide electrolytes, respectively. A three-electrode system was adopted for this experiment, with a carbon rod electrode as the counter electrode, a Hg/Hg_2Cl_2 electrode as the reference electrode, and a carbon paper with the catalyst as the working electrode. A homogeneous ink was prepared by subjecting 4mg of the catalyst powder to ultrasonication in 1mL of deionized water for no less than 30min. Subsequently, the resulting ink was coated onto a carbon fiber paper (CFP) and allowed to air-dry for 1h, achieving a loading density of 0.28mg·cm^{-2}. Then, 0.1 wt % of Nafion (Sigma-Aldrich) was applied to the CFP surface to immobilize the catalyst. All electrodes were connected in a computer-controlled electrochemical workstation (chi660e), and then all data were moderated and detected by the computer. The cyclic activation was run at a scan rate of 100mV·s^{-1} in the potential range of from 1.068 to 2.068V vs. RHE. Linear scanning voltammogram (LSV) scans were maintained at a constant rate of 5mV·s^{-1}. Cyclic durability was checked by timing the ampere response. Electrochemical impedance spectroscopy (EIS) tests were performed at an applied potential of 10mA·cm^{-2} within a frequency range of from 100kHz to 0.1Hz.

3 RESULTS AND DISCUSSION

The preparation process for CoFe PBA composites is illustrated in Figure 1 Initially, solution A was created by combining $Co(NO_3)_2$ and sodium citrate. Concurrently, solution B was prepared by dissolving $K_3Fe(CN)_6$. Subsequently, solution B was introduced to solution A, followed by a thorough mixing and stirring for a duration of 30min. The resulting mixture was then allowed to sit undisturbed for 24h to ensure a complete reaction. During this reaction period, the cobalt ions from $Co(NO_3)_2$ replaced the potassium ions in $K_3Fe(CN)_6$, forming bridging connections with cyanide ligands and Fe^{3+} ions, ultimately leading to the formation of the Co^{2+}-CN-Fe^{3+} structure[18]. The synthesized CoFe PBA composites exhibit a nanocube structure characterized with dark purple color. The subsequent cyclic activation process induced changes in the morphology and composition of PBA, enhancing the presence of active site[19]. As a result, these composites exhibit robust catalytic activity.

SEM images of the CoFe PBA composites were obtained, which clearly illustrate their cubic structure, and the side length is 100-250nm as depicted in Figure 2A. To further affirm the successful preparation of CoFe PBA, we conducted a crystal characterization of the synthesized catalysts using XRD. Figure 2B displays

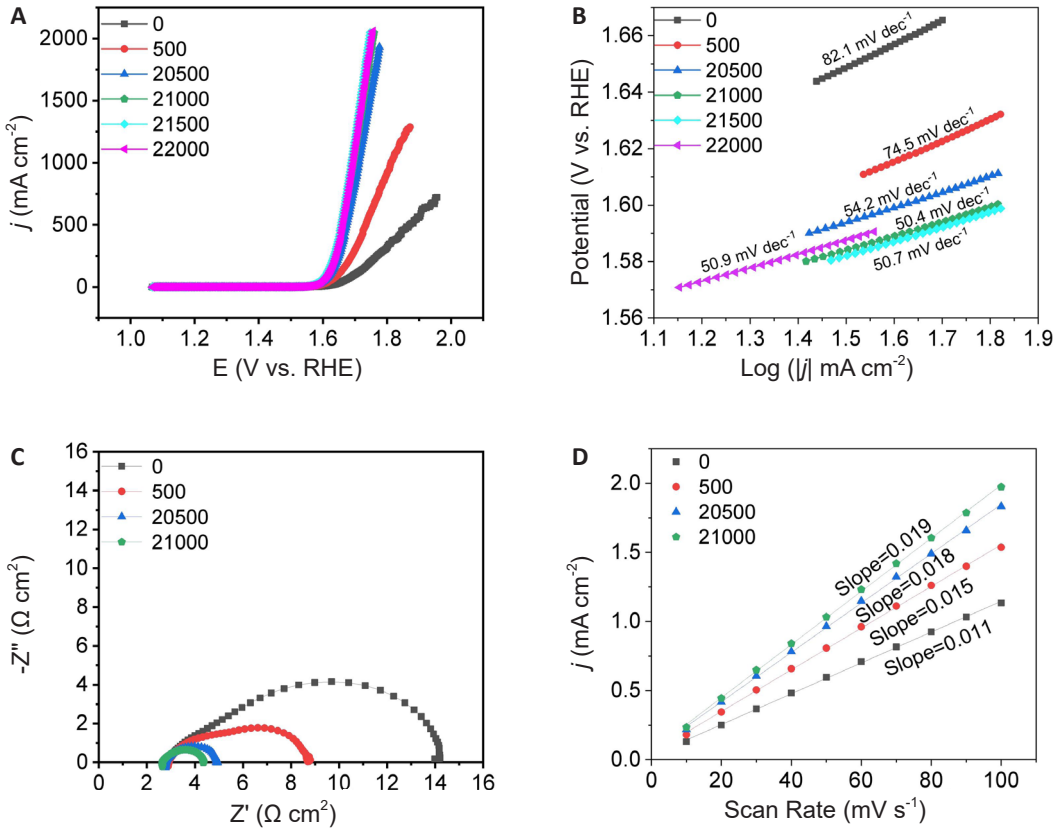

Figure 3. CoFe PBA's OER activity. A: LSV curves of CoFe PBA at the different CV cycling curves; B: the corresponding Tafel slopes; C: EIS curves, D: Cdl curves of CoFe PBA.

four prominent peaks corresponding to the (111), (200), (220), and (400) crystal planes of CoFe PBA. The diffraction patterns observed in CoFe PBA align closely with the known structural properties of CoFe PBA, thereby confirming the successful synthesis of cubic structures of CoFe PBA.

Following the electrochemical treatment through cyclic voltammetry (CV) cycles, the electrocatalytic OER activity of CoFe PBA in a 1M KOH solution was obtained. To provide a comprehensive understanding of CoFe PBA's OER activity after activation, the electrochemical properties of CoFe PBA cycled for 500, 20,500, 21,500 and 22,000 cycles were determined. LSV curves (Figure 3A) revealed that the initial catalyst exhibited poor OER activity, with an initial overpotential reaching as high as 391mV. However, as CV cycling continued, the overpotential progressively decreased. Notably, the sample cycled for 21,000 cycles displayed a significantly lower overpotential of 331mV at a current density of 10mA·cm^{-2} which was lower compared to the uncycled CoFe PBA (391mV), CoFe PBA cycled for 500 (350mV), and CoFe PBA cycled for 20,500 (337mV) electrocatalysts. Moreover, from Figure 3A, it can be seen that the overpotential exhibited a gradual reduction with an increasing number of cycles and there is no significant change after cycling up to 22,000 cycles. The electrocatalysts' OER kinetics were further evaluated through Tafel plots obtained by linearly fitting the polarization curves (Figure 3B). The Tafel slope for the sample cycled 21,000 cycles was the smallest (50.4mV·dec^{-1}), indicating a significant enhancement in CoFe PBA's activity following electrochemical cycling treatment. Moreover, the effect of cycling on the electron transfer capacity of CoFe PBA was investigated using EIS. The EIS data (Figure 3C) demonstrated that cycle-activated CoFe PBA exhibited a lower charge transfer resistance (Rct) compared to the pristine CoFe PBA (uncycled CoFe PBA > CoFe PBA cycled for 500 cycles > CoFe PBA cycled for 20,500 cycles > CoFe PBA cycled for 21,000 cycles), indicating that the surface reconstructed products have better electrical conductivity. Furthermore, the double-layer capacitance (C_{dl}), positively correlated with the electrochemical surface area[20], was extracted from the CV curves at different scan rates (Figure 3D). The C_{dl} values increased in the following order: uncirculated CoFe PBA (11mF·cm^{-2}) < cycled 500 cycles of CoFe PBA (15mF·cm^{-2}) < cycled 20,500 cycles of CoFe PBA (18mF·cm^{-2}) < cycled 21,000 cycles of CoFe PBA (19mF·cm^{-2}), implying an increase in the number of active sites. In summary, these electrochemical results underscore the pivotal role of surface reconstructed in enhancing CoFe PBA's OER performance during the activation process.

To investigate the specific changes in the material's structure before and after cyclic activation, an SEM was used to detect the morphology of catalysts.

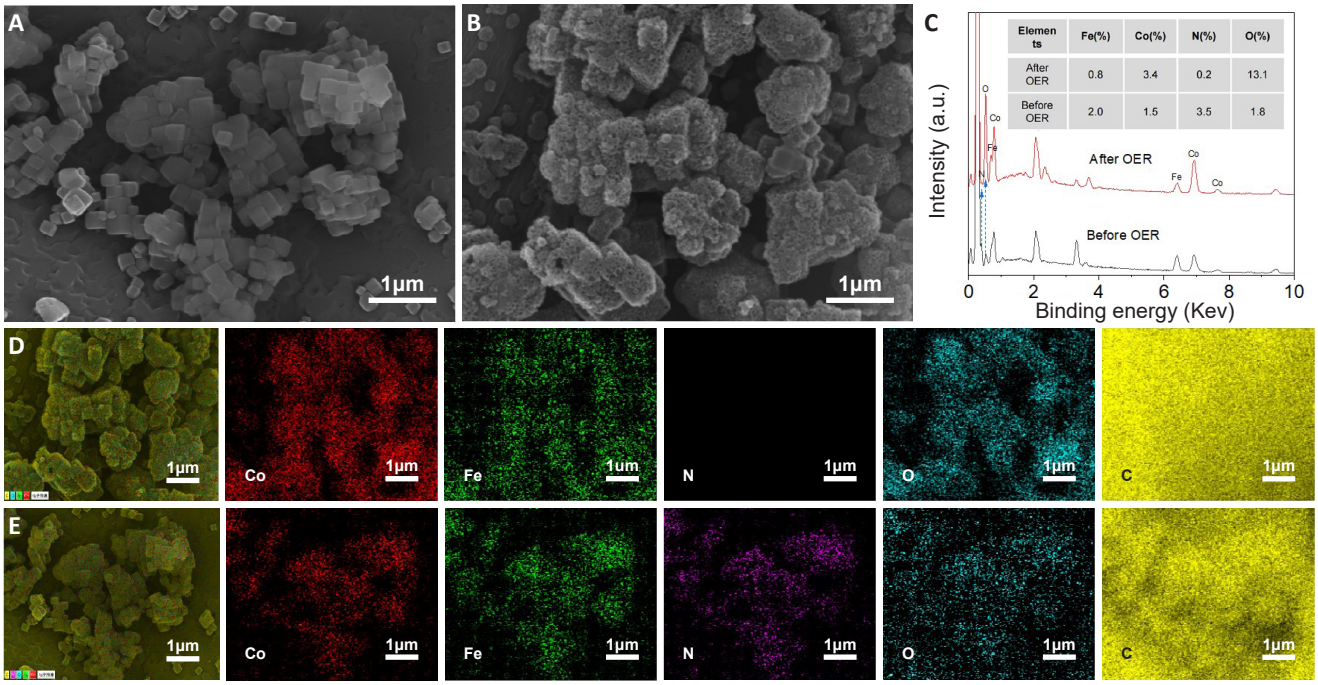

Figure 4. Morphology changes of CoFe PBA. A: SEM image of the initial CoFe PBA; B: SEM image of CoFe PBA after 21000 cycles for OER; C: EDS of before and after CoFe PBA cycles. The inset shows the atomic percentage of the element; D: EDS images for the after CoFe PBA cycle; E: EDS images for the initial CoFe PBA. Bar=1μm (Color in elemental mapping images: red for Co; green for Fe; purple for N; blue for O; yellow for C.)

Figure 4A and 4B vividly illustrate the significant structural transformation in CoFe PBA[21]. After CV cycling for 21,000 cycles, irregular materials proliferated on the surface of the original solid nanocubes, signifying a substantial alteration in the material's structure[22]. Additionally, a comparative analysis of the energy-dispersive spectrometer (EDS) results for CoFe PBA catalysts before and after cyclic activation was conducted. In Figure 4C, through EDS analysis, it is evident that, after CV 21,000 cycles of testing, the oxygen content increased dramatically, reaching 7 times that of the material before cycling, while the nitrogen content saw a significant loss, down to just 1/17 of its initial value. This observation indicates that, during the cycling process, the CoFe PBA underwent an oxidation reaction[23,24]. Notably, after this reaction, the cobalt content doubled compared to its initial state, while the iron content decreased to roughly half of its initial value, suggesting a loss of iron during the in situ reaction. Considering the previously measured performance, it can be inferred that, following 21,000 cycles, the primary active material may be CoOOH[4,19], which aligns with findings in a prior JACS article that discussed NiFe PBA, where nickel served as the active material and Fe ions were lost during the OER process[19]. More interestingly, a porous morphology is observed after the reaction due to the reconstructed structure and the loss of Fe and N. In addition, from the EDS maps in Figure 4D and 4E, it is evident that, initially, the distribution of N is relatively uniform across the material, while the distribution of oxygen (O) is sparse. This suggests that the initial state of the material experiences partial oxidation on the surface. After cycling, the map for cobalt ions (Co) becomes distinct, indicating the dominance of Co elements over Fe elements at this stage. Simultaneously, there is virtually no trace of nitrogen (N), signifying a significant loss of N. Oxygen (O) is clearly visible, predominantly on the material's surface, indicating that a significant portion of the material transformed into oxides or hydroxides[25,26].

To scrutinize the microstructure of the activated catalysts and ascertain their specific compositions, CoFe PBA before cycling, after 500 cycles, and after 21,000 cycles was analyzed and characterized using TEM. As depicted in Figure 5A-C, the catalyst maintains a cubic structure before cycling; upon closer examination, no lattice structures are observed on its surface. This suggests that the catalyst at this stage retains the original cubic structure of CoFe PBA[27]. Figure 5D illustrates that even after 500 cycles, the overall structure of the catalyst maintains its cubic shape. However, Figure 5E clearly shows that the surface of the cube is no longer as smooth as that of the uncycled catalyst[28]. Moreover, visible lattice structures start to emerge on the cube's surface after 500 cycles (Figure 5F)[29]. Furthermore, Figure 5G indicates that the catalyst, after 21,000 cycles, undergoes a significant transformation, losing its cubic structure entirely. Instead, an irregular thin lamellar structure grows on the cube's surface (Figure 5H), and the three-dimensional structure provides and a large surface area[30]. The measured lattice distances of 0.247nm and 0.330nm align

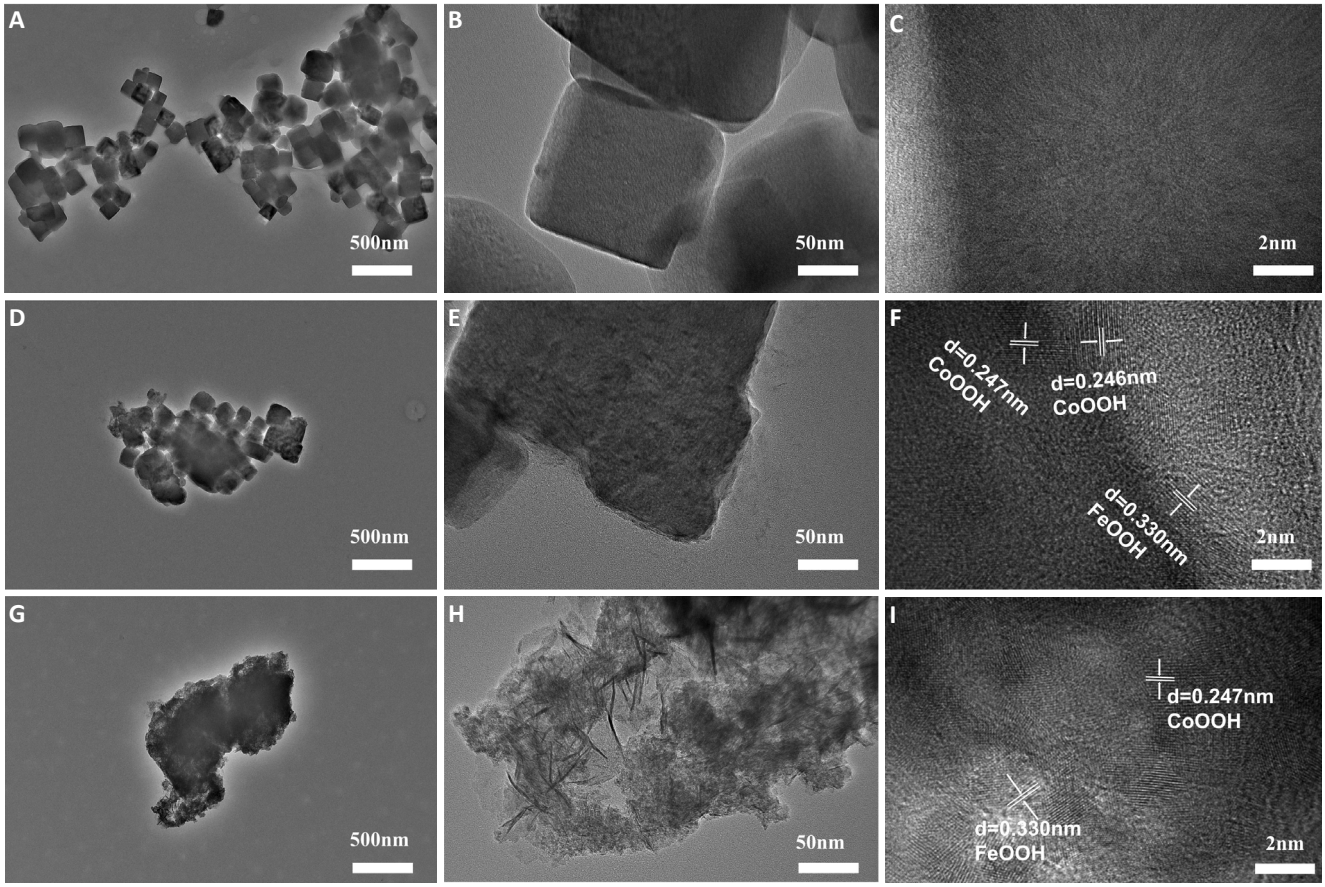

Figure 5. The microstructure changes of CoFe PBA after 500 cycles, and after 21,000 cycles. A-C: TEM patterns of initial CoFe PBA; D-E: TEM patterns of cycled 500 cycles; G-I: TEM patterns of cycled 21,000 cycles.

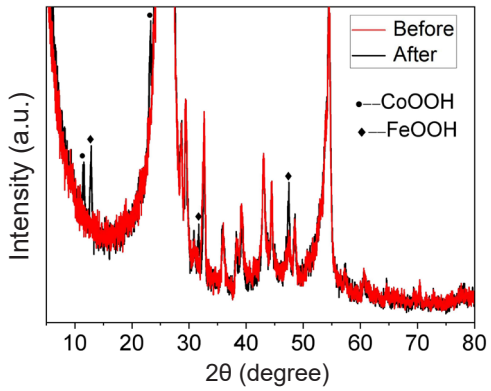

Figure 6. XRD patterns of the before and after CoFe PBA cycle. "Before" represents the results of the catalyst before undergoing cyclic testing, and "after" signifies the results after CV 21,000 cycles of testing.

with those previously reported for CoOOH[31,32] and FeOOH[33]. respectively (Figure 5I). Based on the results above, cyclic activation may lead to the formation of CoOOH and FeOOH.

To pinpoint the specific products resulting from the remodeling of CoFe PBA after cycling, XRD characterizations of CoFe PBA without cycling and following 21,000 cycles of activation were obtained, respectively. It is important to note that, during our sample preparation process, the solution was air-dried by depositing it onto carbon paper, followed by the application of a protective Nafion solution and another round of air-drying. Then, the activation cycling was carried out, and the cyclic material was characterized using XRD on the carbon paper. The XRD analysis can exhibit numerous heterogeneous peaks attributed to carbon and Nafion. After eliminating the carbon peaks, it becomes evident that certain new peaks emerge following the cycling process (Figure 6). These peaks are quite consistent with the previously reported diffraction peaks of CoOOH[31] and FeOOH[34,35], indicating the presence of CoOOH and FeOOH in this catalyst, which is in agreement with the previous TEM observations. Such a phenomenon suggests that CoFe PBA can be activated by oxygen evolution reaction to form the metal hydroxide catalysts CoOOH and FeOOH.

To gain further insight into the specific products of CoFe PBA following OER activation, XPS was employed, as illustrated in Figure 7. The XPS spectra revealed that the CoFe PBA primarily consisted of the elements Co, Fe, C, N, and O, with no presence of other impurities (Figure 7A). In Figure 7B, the two primary XPS peaks at 782.6eV (Co 2p3/2) and 797.9eV (Co 2p1/2) of CoFe PBA without cyclic activation are attributed to Co^{2+}[36,37] and the peaks at 781.4eV and 796.6eV are ascribed to Co^{3+}[38]. In

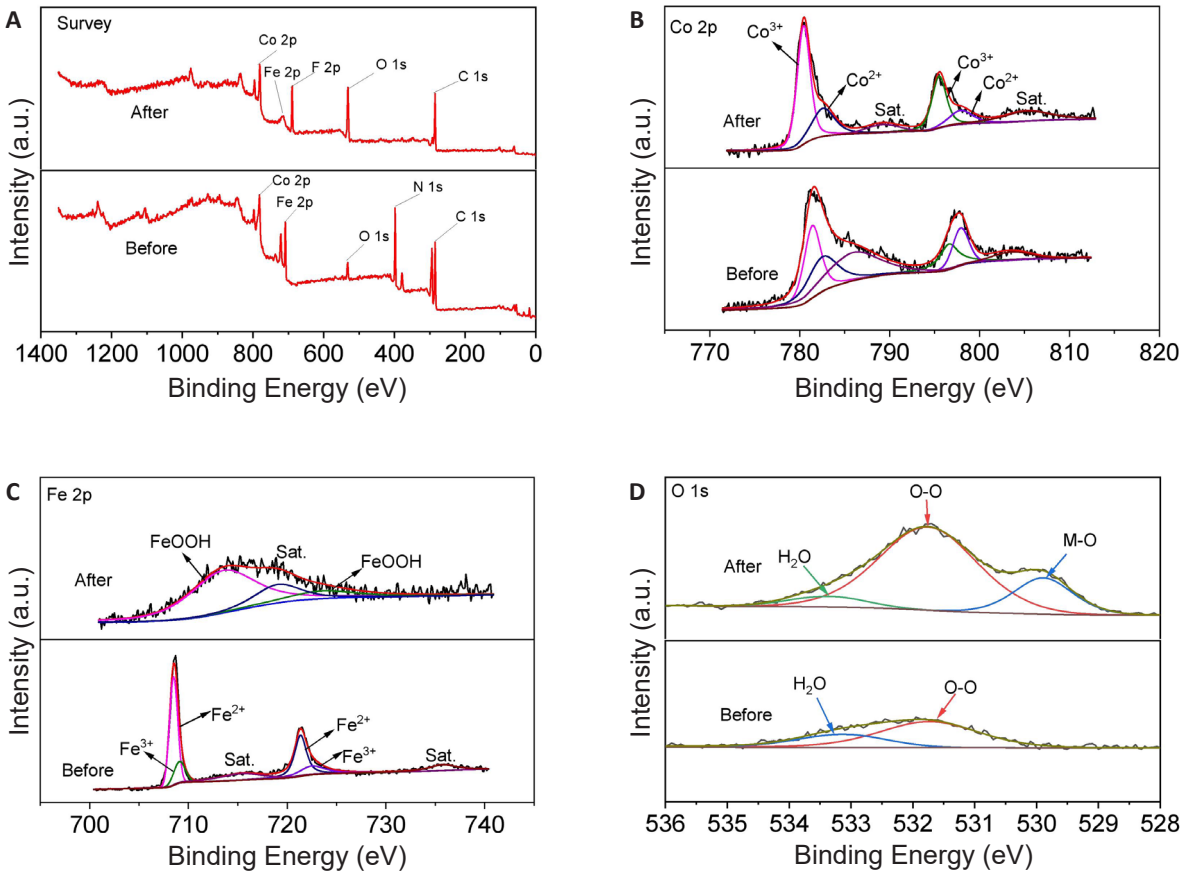

Figure 7. Products of CoFe PBA following OER activation. A: XPS spectra of survey spectrum; B: Co 2p; C: Fe 2p, and D: O 1s for before and after CoFe PBA cycle. Where "before" represents the results of the catalyst before undergoing cyclic testing, and "after" signifies the results after CV 21,000 cycles of testing.

comparison to the original sample, after cycling, the XPS peaks became sharper and more pronounced. The Co 2p show a negative shift suggesting the formation of CoOOH substances[39]. In the XPS analysis of iron (Fe) (Figure 7C), the presence of three peaks at 713.5 and 724.2eV corresponds to the characteristic peaks of Fe 2p1/2 and Fe 2p3/2, in accordance with reported literature on FeOOH[40,41]. In Figure 7D, the intensification of the oxygen (O) peak directly implies the presence of oxide substances, accompanied by the appearance of M-O bonds, signifying the generation of either CoOOH or FeOOH[42]. Based on these results, it is shown that cyclic activation can lead to the remodeling of the CoFe PBA surface.

Figure 8A and 8B illustrate the polarization curves and Tafel slopes of CoFe PBA, Fe-PBA, $Co(OH)_2$, and Pt/C. CoFe PBA after activation exhibits an excellent OER performance, demonstrated by a low overpotential of 331mV at a current density of 10mA cm^{-2} and a small Tafel slope of 50.4mV·dec^{-1}, surpassing that of $Co(OH)_2$ (386mV/80.7mV·dec^{-1}) and Fe-PBA (360mV/60.9mV·dec^{-1}), and comparable to commercial Pt/C (410mV/124mV·dec^{-1}). EIS was conducted, as depicted in Figure 8C, and CoFe PBA exhibited a lower electron transfer resistance compared to pristine $Co(OH)_2$, Fe-PBA and Pt/C. This suggests more efficient electron transport and enhanced OER kinetics in CoFe PBA. It is noteworthy that the CoFe PBA catalyst exhibited remarkable long-term stability during the assessment. After 37h of continuous testing at current densities of 10mA·cm^{-2}, the catalyst displayed negligible activity decay, as depicted in Figure 8D. By electrochemical oxidation, the CoFe PBA surfaces partially reconstitute CoOOH and FeOOH which serve as highly active catalysts for the OER, contributing to the sustained catalytic performance of CoFe PBA[43-47].

4 CONCLUSIONS

Our research underscores the critical importance of developing highly efficient catalysts for OER to advance electrochemical conversion technologies. Through electrochemical oxidation, the electrocatalytic performance of CoFe PBA was substantially enhanced. After 21,000CV cycles of testing, the CoFe PBA exhibits outstanding characteristics, including a low overpotential of 331mV at a current density of 10mA·cm^{-2}, a small Tafel slope of 50.4mV·dec^{-1}, and exceptional long-term stability during electrolysis in a 1M KOH alkaline medium for over 37h. These findings demonstrate the potential of CoFe PBA as a promising

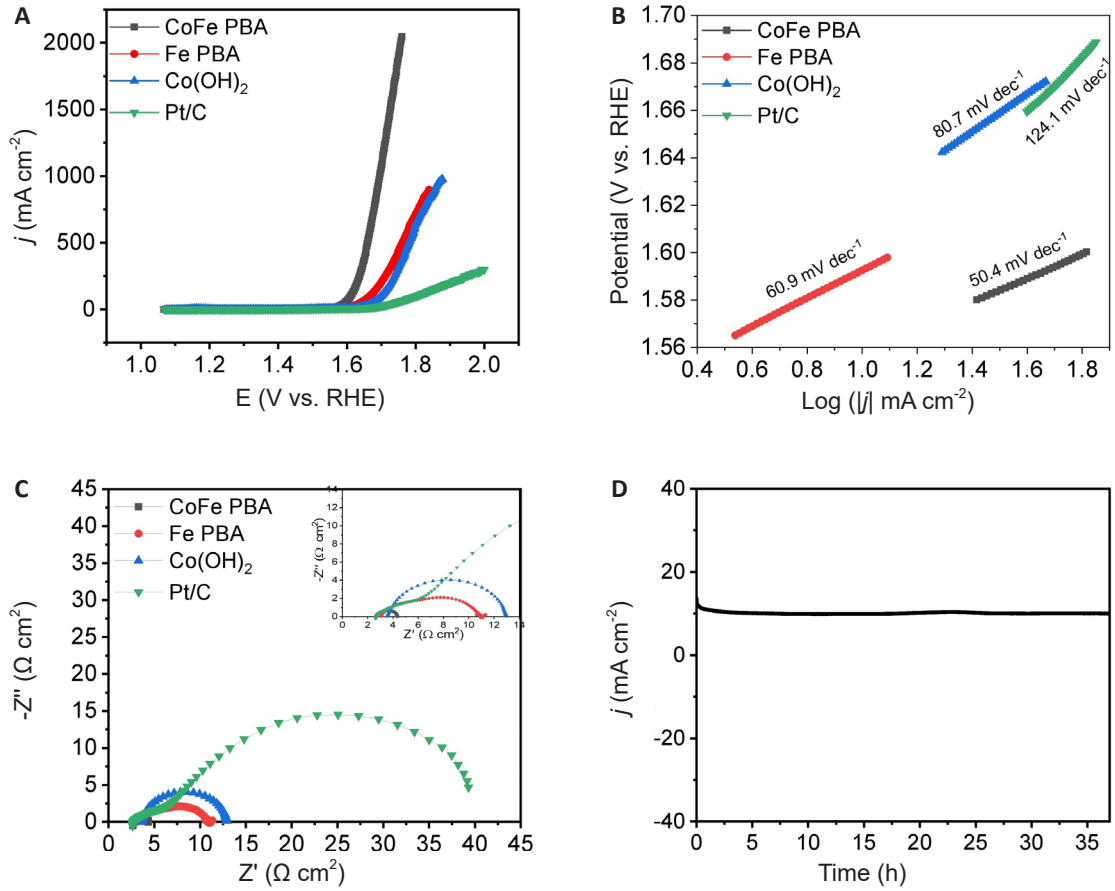

Figure 8. CoFe PBA after activation exhibits an excellent OER performance. A: LSV curves; B: Tafel slopes images; C: EIS curves of CoFe PBA, Fe PBA, Co $(OH)_2$, and Pt/C, and the current density-time curves; D: of CoFe PBA.

OER catalyst. This is attributed to the conversion of CoFe PBA into CoOOH and a minor proportion of FeOOH during the oxidation reaction, which serve as the active sites for OER.

Acknowledgements

Acknowledgements are extended to the Basic Scientific Research Project of the Education Department of Liaoning Province (Grant No. LJKMZ20220739 and JYTMS20231430), Creative Project of Engineering Research Center of Alternative Energy Materials & Devices, Ministry of Education, Sichuan University (Grant NO. AEMD202205), and the Research Foundation of Liaoning Petrochemical University (Grant No. 2019XJJL-022), Yunnan Provincial Rural Energy Engineering Key Laboratory (2022KF005) for their valuable support.

Conflicts of Interest

There are no conflicts to declare.

Author Contribution

Huang C conceived the original concept and designed the experiments. Chen Y conducted the electrochemical measurements and analysis. Tu J contributed to the XPS measurements and analyzed the results. Li W performed the EDS, XRD, and TEM characterizations. Tang J wrote the paper. Huang C and Li W revised and edited the manuscript. Li W coordinated and supervised the research. All authors contributed to writing the manuscript.

Abbreviation List

CFP, Carbon fiber paper
CoFe PBA, Co-Fe Prussian blue analogue
CV, Cyclic voltammetry
EDS, Energy-dispersive spectrometer
EIS, Electrochemical impedance spectroscopy
HER, Hydrogen evolution reaction
LSV, Linear scanning voltammogram
OER, Oxygen evolution reaction
PBAs, Prussian blue analogues
SEM, Scanning electron microscope
TEM, Transmission electron microscope
XPS, X-ray photoelectron spectroscopy
XRD, Powder X-ray diffraction

References

[1] Tran VA, Do HH, Vasseghian Y et al. Metal-organic-framework-derived metals and metal compounds as electrocatalysts for oxygen evolution reaction: A review. *Int J Hydrog Energy*, 2022; 47: 19590-19608.[DOI]

[2] Ehlers JC, Feidenhans'l AA, Therkildsen KT et al. Affordable Green Hydrogen from Alkaline Water Electrolysis: Key Research Needs

from an Industrial Perspective. *ACS Energy Lett*, 2023; 8: 1502-1509. [DOI]

[3] Kahlstorf T, Hausmann JN, Sontheimer T et al. Challenges for Hybrid Water Electrolysis to Replace the Oxygen Evolution Reaction on an Industrial Scale. *Glob Chall*, 2023; 7: 2200242.[DOI]

[4] Huang C, Qin P, Luo Y et al. Recent progress and perspective of cobalt-based catalysts for water splitting: design and nanoarchitectonics. *Mater Today Energy*, 2022; 23: 100911.[DOI]

[5] Audichon T, Napporn TW, Canaff C et al. IrO_2 Coated on RuO_2 as Efficient and Stable Electroactive Nanocatalysts for Electrochemical Water Splitting. *J Phys Chem C*, 2016; 120: 2562-2573.[DOI]

[6] Li C, Baek JB. Recent Advances in Noble Metal (Pt, Ru, and Ir)-Based Electrocatalysts for Efficient Hydrogen Evolution Reaction. *ACS Omega*, 2020; 5: 31-40.[DOI]

[7] Roca-Ayats M, Herreros E, García G et al. Promotion of oxygen reduction and water oxidation at Pt-based electrocatalysts by titanium carbonitride. *App Catal B*, 2016; 183: 53-60.[DOI]

[8] Shi Q, Zhu C, Du D et al. Robust noble metal-based electrocatalysts for oxygen evolution reaction. *Chem Soc Rev*, 2019; 48: 3181-3192.[DOI]

[9] Huang C, Zhang XL, Tang J et al. Spatially strain-induced and selective preparation of Mo_xN (x = 1, 2) as a highly effective nanoarchitectonic catalyst for hydrogen evolution reaction in a wide pH range. *Rare Metals*, 2023; 42: 1446-1452.[DOI]

[10] Hughes JP, Clipsham J, Chavushoglu H et al. Rowley-Neale and C.E. Banks, Polymer electrolyte electrolysis: A review of the activity and stability of non-precious metal hydrogen evolution reaction and oxygen evolution reaction catalysts. *Renew Sust Energ Rev*, 2021; 139: 110709.[DOI]

[11] Tang J, Huang C, Wu Q et al. Atomic-scale intercalation of N-doped carbon into monolayered $MoSe_2$-Mo_2C heterojunction as a highly efficiency hydrogen evolution reaction catalyst, *J Electroanal Chem*. 2022; 906: 115897.[DOI]

[12] Zhang W, Zhao Y, Malgras V et al. Synthesis of monocrystalline nanoframes of prussian blue analogues by controlled preferential etching. *Angew Chem Int Ed*, 2016; 55: 8228-8234.[DOI]

[13] Diao F, Kraglund MR, Cao H et al. Moderate heat treatment of CoFe Prussian blue analogues for enhanced oxygen evolution reaction performance. *J Energy Chem*, 2023; 78: 476-486.[DOI]

[14] Lu X, Xu H, Yang T et al. Co^{3+}-rich CoFe PBA encapsulated in ultrathin MoS_2 sheath as integrated core-shell architectures for highly efficient OER. *J Alloys Compd*, 2023; 942: 169004.[DOI]

[15] Zeng C, Li Q, You Y et al. Structural regulation of Fe–Co prussian blue analogues by incorporation of Pt for enhanced electrocatalytic overall water splitting. *Int J Hydrog Energy*, 2022; 47: 35149-35155. [DOI]

[16] Rodríguez-García B, Reyes-Carmona Á, Jiménez-Morales I et al. Cobalt hexacyanoferrate supported on Sb-doped SnO_2as a non-noble catalyst for oxygen evolution in acidic medium. *Sustain Energy Fuels*, 2018; 2: 589-597.[DOI]

[17] Zhao G, Wang B, Yan Q et al. Mo-doping-assisted electrochemical transformation to generate CoFe LDH as the highly efficient electrocatalyst for overall water splitting. *J Alloys Compd.*, 2022; 902: 163738.[DOI]

[18] Zhu P, Li X, Yao H et al. Hollow cobalt-iron prussian blue analogue nanocubes for high-performance supercapacitors. *J Energy Storage*, 2020; 31: 101544.[DOI]

[19] Su X, Wang Y, Zhou J et al. Operando spectroscopic identification of active sites in nife prussian blue analogues as electrocatalysts: Activation of oxygen atoms for oxygen evolution reaction. *J Am Chem Soc*, 2018; 140: 11286-11292.[DOI]

[20] Huang C, Chu PK. Recommended practices and benchmarking of foam electrodes in water splitting. *Trends Chem*, 2023; 5: 242-243. [DOI]

[21] Chen J, Chen H, Yu T et al. Recent Advances in the Understanding of the Surface Reconstruction of Oxygen Evolution Electrocatalysts and Materials Development. *Electrochem Energy Rev*, 2021; 4: 566-600. [DOI]

[22] Gupta PK, Sharma GP, Pala RGS. Surface-enhanced OER activity in $Co_3V_2O_8$ using cyclic charge-discharge to balance electrocatalytic active site generation and degradation. *Electrochim Acta*, 2021; 367: 137538.[DOI]

[23] Kudielka A, Bette S, Dinnebier RE et al. Variability of composition and structural disorder of nanocrystalline CoOOH materials. *J Mater Chem C*, 2017; 5: 2899-2909.[DOI]

[24] Li X, Graham NJD, Deng W et al. The formation of planar crystalline flocs of gamma-FeOOH in Fe(II) coagulation and the influence of humic acid. *Water Res*, 2020; 185: 116250.[DOI]

[25] Chen W, Wang H, Li Y et al. In situ electrochemical oxidation tuning of transition metal disulfides to oxides for enhanced water oxidation. *ACS Cent Sci*, 2015; 1: 244-51.[DOI]

[26] Liu Y, Wang S, Li Z et al. Insight into the surface-reconstruction of metal–organic framework-based nanomaterials for the electrocatalytic oxygen evolution reaction. *Coord Chem Rev*, 2023; 484: 215117.[DOI]

[27] Du Y, Chen J, Li L et al. Core–Shell FeCo Prussian Blue Analogue/$Ni(OH)_2$ Derived Porous Ternary Transition Metal Phosphides Connected by Graphene for Effectively Electrocatalytic Water Splitting. *ACS Sustain Chem Eng*, 2019; 7: 13523-13531.[DOI]

[28] Huang C, Zhang B, Wu Y et al. Experimental and theoretical investigation of reconstruction and active phases on honeycombed Ni_3N-Co_3N/C in water splitting. *Appl Catal B*, 2021; 297: 120461. [DOI]

[29] Dutta A, Samantara AK, Dutta SK et al. Surface-oxidized dicobalt phosphide nanoneedles as a nonprecious, durable, and efficient OER catalyst. *ACS Energy Lett*, 2016; 1: 169-174.[DOI]

[30] Huang C, Miao X, Pi C et al. Mo_2C/VC heterojunction embedded in graphitic carbon network: An advanced electrocatalyst for hydrogen evolution. *Nano Energy*, 2019; 60: 520-526.[DOI]

[31] Huang J, Chen J, Yao T et al., CoOOH nanosheets with high mass activity for water oxidation. *Angew Chem Int Ed Engl*, 2015; 54: 8722-8727.[DOI]

[32] Wang H, Zhou Y, Tao S. CoP-CoOOH heterojunction with modulating interfacial electronic structure: A robust biomass-upgrading electrocatalyst. *Appl Catal B*, 2022; 315: 121588.[DOI]

[33] Yin H, Gao X, Chen P. One-step synthesis of FeO(OH) nanoparticles by electric explosion of iron wire underwater, *Def Technol*, 2022; 18: 133-139.[DOI]

[34] Mahasti NNN, Shih YJ, Huang YH. Removal of iron as oxyhydroxide (FeOOH) from aqueous solution by fluidized-bed homogeneous crystallization. *J Taiwan Inst Chem Eng*, 2019; 96: 496-502.[DOI]

[35] Sugae K, Kamimura T, Asakura R et al. Electrochemical reduction and re-oxidation behavior of α, β, and γ-iron oxy-hydroxide films on electrodes. *Mater Corros*, 2018; 70: 187-196.[DOI]

[36] Huang C, Wu D, Qin P et al. Ultrafine Co nanodots embedded in N-doped carbon nanotubes grafted on hexagonal VN for highly efficient overall water splitting. *Nano Energy*, 2020; 73: 104788. [DOI]

[37] Le K, Gao M, Liu W et al. MOF-derived hierarchical core-shell hollow iron-cobalt sulfides nanoarrays on Ni foam with enhanced electrochemical properties for high energy density asymmetric supercapacitors. *Electrochim Acta*, 2019; 323: 134826.[DOI]

[38] Fan K, Zou H, Lu Y et al. Direct observation of structural evolution of metal chalcogenide in electrocatalytic water oxidation. *ACS Nano*, 2018; 12: 12369-12379.[DOI]

[39] Tang J, Wan W, Liu S et al. Activating Co sites activity in $Co(OH)_2$ via VN coupling to facilitate highly efficient oxygen evolution reaction. *Int J Hydrog Energy*, 2024; 56: 242-247.[DOI]

[40] Li J, Xu Y, Zhang Y et al. Enhanced redox kinetics of polysulfides by nano-rod FeOOH for ultrastable lithium–sulfur batteries. *J Mater Chem A*, 2020; 8: 19544-19554.[DOI]

[41] Tao R, Qu M, Zhang S et al. Preparation of FeOOH supported by melamine sponge and its application for efficient phosphate removal. *J Environ Chem Eng*, 2022; 10: 108064.[DOI]

[42] Zhu M, Zhao B, Yuan Y et al. Study on corrosion behavior and mechanism of CoCrFeMnNi HEA interfered by AC current in simulated alkaline soil environment. *J Electroanal Chem*, 2021; 882: 115026.[DOI]

[43] Indra A, Paik U, Song T. Boosting electrochemical water oxidation with metal hydroxide carbonate templated prussian blue analogues. *Angew Chem Int Ed Engl*, 2018; 57: 1241-1245.[DOI]

[44] Liu T, Li P, Yao N et al. Self-Sacrificial Template-Directed Vapor-Phase Growth of MOF Assemblies and Surface Vulcanization for Efficient Water Splitting. *Adv Mater*, 2019; 31: 1806672.[DOI]

[45] Pintado S, Goberna-Ferrón S, Escudero-Adán EC et al. Fast and persistent electrocatalytic water oxidation by Co-Fe Prussian blue coordination polymers. *J Am Chem Soc*, 2013; 135: 13270-13273.[DOI]

[46] Qian Q, Li Y, Liu Y et al. Ambient fast synthesis and active sites deciphering of hierarchical foam-like trimetal-organic framework nanostructures as a platform for highly efficient oxygen evolution electrocatalysis. *Ad. Mater*, 2019; 31: 1901139.[DOI]

[47] Wang Y, Ma J, Wang J et al. Interfacial scaffolding preparation of hierarchical pba-based derivative electrocatalysts for efficient water splitting. *Adv Energy Mater*, 2019; 9: 1802939.[DOI]

Brief of Corresponding Author(s)

Chao Huang

He is a Postdoctoral Fellow under the supervision of Prof. Paul K. Chu. He received his PhD from City University of Hong Kong in 2021. He received his MS and BS from Wuhan University of Science and Technology in 2017 and 2014, respectively. His research focuses on synthesis of functional nanomaterials and their applications in energy storage and conversion. His h-index is 33 in March 2024.